Application of Work-of-Sintering Concepts in Powder Metals

DEBORAH C. BLAINE, SEONG JIN PARK, PAVAN SURI, and RANDALL M. GERMAN

One of the current challenges facing the particulate materials industry is developing simple, accurate models to predict sintered properties. Work-of-sintering concepts, where time-temperature integrals are used in such models, offer a solution to this problem. In this study, the master sintering curve concept is applied to several powder metal systems: 17 to 4PH stainless steel, 316L stainless steel, nickel, niobium, tungsten heavy alloys with two different compositions, and molybdenum. A detailed explanation of the construction of these curves is given, including methods used to calculate the apparent activation energy for sintering and to curve-fit experimental data to a sigmoid function describing the master sintering curve. Discussion of the results shows that the master sintering curve can be applied to powder metal systems, even those that use liquid phase during sintering.

I. INTRODUCTION

TRADITIONALLY, the reaction rate of thermally activated kinetic processes is best described through exponential temperature dependence. The Arrenhius equation is a favored form where the exponent includes an activation energy for the reaction.[1] This concept has been widely applied to models describing sintering, a thermally activated process that usually occurs due to diffusion processes.[2,3,4] Diffusion itself is described by the Arrenhius temperature dependence. An additional concept, the work of sintering, evolved from this treatment of sintering where the sintered properties are related to a single time-temperature integral.[5] This concept is the same as the master sintering curve developed by Su and Johnson.[6,7] Shercliff and Ashby used a similar time-temperature integral to describe the annealing recovery of aluminum alloys.[8]

The master sintering curve has been studied for a number of ceramic systems such as alumina and yittria-stabilized zirconia.[7,9] Teng *et al.*,[10] developed a computer program to construct the master sintering curve from experimental data for yittria-stabilized zirconia (5 wt pct yittria), fitting a sigmoid function between the relative density data and the natural logarithm of the work of sintering. The master sintering curve approach was used to determine the activation energy for sintering of ThO_2-U_3O_8 fuel pellets, used in advanced heavy water reactors.[11]

In this article, we use similar methods to construct master sintering curves relating sintered density to the work of sintering for several powder metal systems: 17-4 PH stainless steel, 316L stainless steel, tungsten heavy alloys, molybdenum, niobium, and nickel. We found that in order to accurately determine the activation energy for sintering, a normalized dimensionless mean square residual had to be used. Additional details on extracting density directly from dilatometry data are given. We show that the work of sintering concept can be applied to powder metal systems through the master sintering curve; however, there are some limitations and conditions pertaining to its use.

DEBORAH C. BLAINE, Deputy Manager, Materials Research and Development, is with Bleistahl Produktions GmbH & Co. KG, Wetter D-58300, Germany. Contact e-mail: d.blaine@bleistahl.de SEONG JIN PARK, Research Professor, and RANDALL M. GERMAN, CAVS Chair Professor of Mechanical Engineering and Director, are with the Center for Advanced Vehicular Systems, Mississippi State University, Mississippi State, MS 39762-5404. PAVAN SURI, Senior Research Scientist, is with the Production Engineering Research Lab, Matsushita Electric Works Ltd., Osaka 5718686, Japan.

Manuscript submitted January 13, 2006.

II. THEORY OF MSC

Sintering of particulate materials is a thermally activated process involving mass-transport events that results in particle bonding.[12] These mass-transport events work to reduce the free surface area of the compact. Surface transport mechanisms work only to grow the sinter bond between particles, while bulk transport mechanisms work to draw the particle centers together, thus increasing the density of the porous body while simultaneously reducing the free surface energy. Associated with this sintering densification is a decrease in volume, so by measuring dimensional changes during sintering, the change in density can be monitored. Through extensive studies on the mass-transport mechanisms resulting in densification, a combined stage sinter model was developed that predicts the dimensional and density changes that take place during sintering.[13] The compact densification is linked to the dominant diffusional events that occur, grain boundary and volume diffusion, resulting in the following combined-stage sintering equation:

$$-\frac{dL}{L\,dt} = \frac{\gamma\Omega}{kT}\left[\frac{\Gamma_V D_V}{G^3} + \frac{\Gamma_b D_b}{G^4}\right] \qquad [1]$$

where L is the dimension of the compact, t is time, γ is the surface energy, Ω is the atomic volume, k is Boltzmann's constant, T is the temperature, Γ is a lumped scaling factor, D is the diffusivity, G is the grain size, and the subscripts v and b refer to volume diffusion and grain boundary diffusion, respectively.

For isotropic shrinkage, the sintering shrinkage rate can be linked to the densification rate by considering the conservation of mass, resulting in the following approximate relationship:

$$-\frac{dL}{L\,dt} = \frac{d\rho}{3\rho\,dt} \qquad [2]$$

Combining Eqs. [1] and [2] provides a link between densification rate and diffusional sintering events. However,

the lumped scaling factors Γ are arbitrary parameters containing density-dependent geometric terms.[9] Furthermore, the diffusivities for grain boundary and volume diffusion D vary significantly between studies,[14] so no reliable value can be assigned with confidence to a particular material. Thus, determination of the shrinkage and densification rates from the combined-stage sinter model requires experimental characterization of the lumped scaling factors and diffusivities for specific sintering systems. To overcome this challenge, the combined-stage sintering equation was rearranged by Su and Johnson[6] with all of the density ρ-dependent material parameters grouped on one side, and the known process-dependent parameters, with the exception of the apparent activation energy Q, grouped on the other side as follows:[7]

$$\int_{\rho_0}^{\rho} \frac{kG^n}{3\rho\gamma\Omega D_0\Gamma} d\rho = \int_{t_0}^{t} \frac{1}{T} \exp\left(-\frac{Q}{RT}\right) dt \qquad [3]$$

where D_0 is the diffusivity pre-exponent. The diffusivities as given in Eq. [1] follow Arrenhius temperature dependence and have been broken up into their pre-exponential and exponential terms in Eq. [3]. As grain boundary and volume diffusion have varying relative influences on the densification response of a sintering system, they have been lumped together as an apparent diffusivity in Eq. [3] to create a master sintering curve. The rearranged combined-stage sintering model is integrated from the initial time and density values, indicated by the subscript o, to any point (t, T, ρ) during thermal processing.

The right-hand side of Eq. [3] is calculated through numerical integration and represents a measure of the energy supplied to the system during nonisothermal sintering. Thus, the term work of sintering Θ is applied to this expression, giving

$$\Theta(t,T) = \int_{t_0}^{t} \frac{1}{T} \exp\left(-\frac{Q}{RT}\right) dt \qquad [4]$$

The apparent activation energy for sintering in Eq. [4] is found through numerical analysis, as explained further on. For any work of sintering value, there is a corresponding density condition that satisfies Eq. [3] for a given system. Thus, once the relationship between density and work of sintering is established, a master sintering curve describing this relationship is determined for a given sintering system.

III. EXPERIMENTAL PROCEDURES

A. *Sample Materials*

For this study, seven powder systems were examined, as listed in Table I. Details of the sample preparation and the sintering tests performed follow. In all cases, only the mean particle size was given because the purpose of this study is to show the efficacy of the master sintering curve as a model over a range of powders and materials, and not to characterize highly specialized models for specific particle size distributions. However, it should be noted that particle size distribution should be taken into account for improved accuracy in the model. Dilatometry, the experimental measurement of *in-situ* sintering shrinkage, was conducted using a vertical pushrod dilatometer (Anter Corporation, Pittsburgh, PA).

1. *17-4 PH stainless steel*

Water-atomized powder (ATMIX Corp., Aomori, Japan; mean particle size of 7.6 μm), mixed with a water-based agar binder at 55 vol pct solids loading, was injection molded into tensile bars.[15] Due to the nature of the binder, the samples did not require a solvent debind step. Thermal debinding was performed in a retort furnace in hydrogen under the following thermal cycle: ramp at 2 °C/min with intermediate 2-hour holds at 60 °C, 110 °C, and 450 °C. The initial density remained unchanged at 55 pct of the theoretical density after debinding. Dilatometry was performed on debound samples, and run in a hydrogen atmosphere using the following thermal cycle: ramp at 10 °C/min to 1010 °C, hold for 1 hour, ramp at 1.67 °C/min to 1330 °C for one experiment and 1365 °C for another, with a 1-hour hold at the peak temperature. A third experiment was run with a 10 °C/min ramp to 1200 °C with no hold.

2. *316L stainless steel*

Die compaction grade, water-atomized 316L stainless steel (Ametek, Wallingford, CT; mean particle size of 37.9 μm), mixed with 1 wt pct Acrawax, was compacted into 12.5-mm-diameter cylinders with density 6.4 g/cm^3. Dilatometry was performed in hydrogen under the following thermal cycles: ramp at 10 °C/min to 1150 °C or 1300 °C with a 1-hour hold at temperature. Figure 1(a) shows the densification curves calculated from the dilatometry data of these tests.

3. *95 pct tungsten heavy alloy*

Premixed W-Ni-Fe powders (HC Starck/Kulite, Newton, MA, 95 wt pct W, 3.5 wt pct Ni, 1.5 wt pct Fe; mean particle size of 7.6 μm), mixed with a water-based agar binder at 55 vol pct solids loading, was injection molded

Table I. Samples and Test Methods for Construction of Master Sintering Curve

Materials	Sample Preparation	Debinding/Delubrication	Initial Relative Density	Test Method
17-4PH SS	PIM with agar binder	thermal	0.55	dilatometry
316L SS	compaction	thermal	0.81	dilatometry
W-Ni-Fe (95:3:2)	PIM with agar binder	thermal	0.50	dilatometry
W-Ni-Fe (88:8.4:3.6)	CIP	thermal	0.65	dilatometry
niobium	PIM with wax-polymer binder	solvent/thermal	0.57	Archimedes
molybdenum	PIM with wax-polymer binder	solvent/thermal	0.52	Archimedes
nickel	PIM with wax-polymer binder	solvent/thermal	0.60	dilatometry

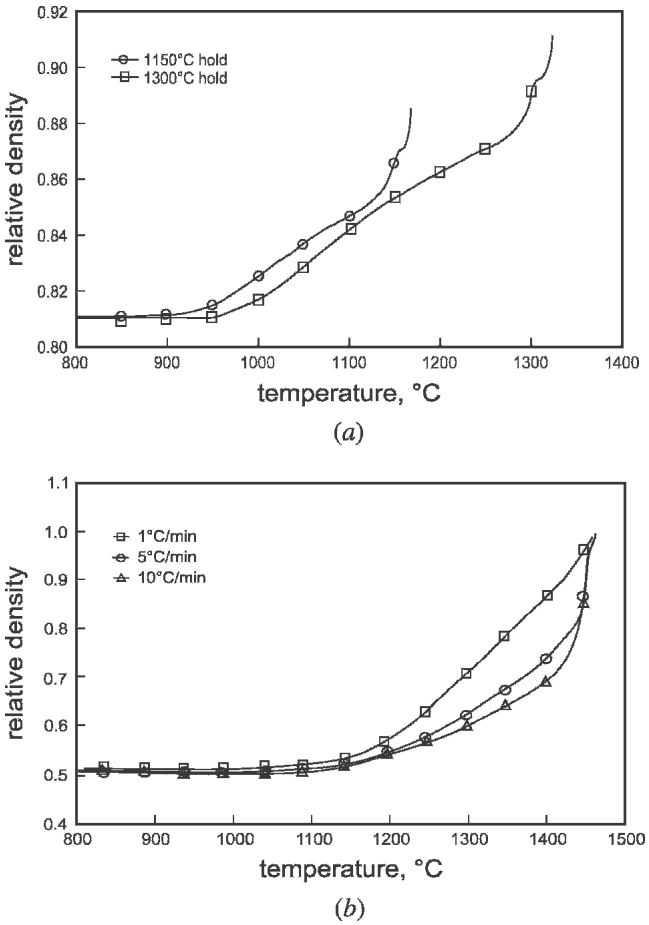

Fig. 1—Dilatometry data for (*a*) 316L stainless steel and (*b*) W-Ni-Fe (95:3:2).

into tensile bars. Samples for dilatometry were cut from the gate sections and thermally debound in hydrogen using the following thermal cycle: ramp at 2 °C/min with intermediate 2-hour holds at 60 °C, 110 °C, and 450 °C. The density after debinding was measured as 50 pct of the theoretical density. The thermal cycles used for dilatometry, performed in hydrogen, were ramp at 10 °C/min to 900 °C, hold for 1 hour, ramp at either 1 °C, 5 °C, or 10 °C/min to 1460 °C, hold for 30 minutes. Figure 1(b) shows the densification curves calculated from the dilatometry data of these tests.

4. *88 pct tungsten heavy alloy*

The alloy was formed from an elemental mixture of three powders: rod-milled tungsten powder (Osram Sylvania, Towanda, PA; mean particle size of 3 μm), carbonyl nickel powder (Novamet INCO, Wyckoff, NJ; mean particle size of 10 μm), and carbonyl iron powder (ISP INCO, Wyckoff, NJ; mean particle size of 6 μm). The weight ratio of powders was 88:8.4:3.6 W:Ni:Fe, with the nickel-to-iron ratio 7:3 to avoid the formation of intermetallics during sintering. The mixed powder was cold isostatic pressed (CIP) at 280 MPa into rods of about 10.6-mm diameter, with green density between 64 and 68 pct of the theoretical density. The green rods were cut into samples of 10-mm height. Dilatometry was performed on the samples in hydrogen under the following thermal cycle: 10 °C/min ramp to 900 °C, with a 1-hour hold to remove oxides, continued 10 °C/min ramp to 1400 °C, with a 5-minute hold to stabilize at this temperature. From 1400 °C to 1500 °C, ramp rates of 1 °C/min, 5 °C/min, 10 °C/min, and 15 °C/min were used for different experiments, all of the experiments held at 1500 °C for 30 minutes.[16]

5. *Niobium*

Niobium powder (Cabot Corp., Albuquerque, NM; mean particle size of 7.5 μm), compounded at 57 vol pct solids loading with a wax-polymer binder, was injection molded into tensile bars. The samples were solvent debound in a heptane bath at 60 °C for 2 hours. Following solvent debinding, the samples were thermally debound and presintered in a retort furnace in pure hydrogen under the following thermal cycle: a 5 °C/min ramp with intermediate 1-hour holds at 260 °C, 440 °C, and 1150 °C. Sintering was performed in three different furnaces. In the first furnace, the samples were sintered under $1.3 \cdot 10^{-4}$ Pa vacuum to 1600 °C for 1, 1.5, and 2 hours. The second furnace was a graphite vacuum furnace operating under 0.13 Pa vacuum. The samples were sintered to 1600 °C for 1 hour, 1800 °C for 1 hour, or 2000 °C for 2 or 0.5 hours. The third set of sintering experiments was conducted in a continuous graphite belt furnace operating at very low partial pressure of oxygen. The thermal cycles used were 1600 °C for 1.5 hours, 1800 °C for 2 hours, and 2000 °C for 1.5 hours.[17] Densities of the sintered samples were measured using the Archimedes technique.

6. *Molybdenum*

Injection molding grade molybdenum powder (HC Starck, Newton, MA), mixed at 60 vol pct solids loading with a wax-polymer binder, was injection molded into bars. The samples were solvent debound in heptane at 60 °C. This was followed by thermal debinding and presintering, to remove contaminants, in hydrogen. The samples were then sintered in a graphite element vacuum furnace (0.13 Pa) using the following thermal cycles: ramp at 1 °C/min, 2 °C/min, or 5 °C/min to peak temperatures of 1600 °C, 1700 °C, or 1800 °C with 1-, 2-, or 10-hour holds at temperature.[18] The sintered density of the samples was measured using the Archimedes water-immersion technique.

7. *Nickel*

Carbonyl nickel powder (Novamet 4SP-10 μm, INCO, Wyckoff, NJ), compounded at 60 vol pct solids loading with a wax-polymer binder, was injection molded into rectangular bars.[19] A bar was cut along its length into samples about 7-mm wide. The samples were debound and presintered in a retort furnace in hydrogen using the following thermal debind cycle: 2 °C/min to 475 °C, hold for 4 hours. Dilatometry was performed in hydrogen on the samples under the following thermal cycle: ramp at 5 °C/min to 1100 °C, hold for 1 hour.

Table I shows a summary of the materials and corresponding sample preparation and experiments performed in this study.

B. *Treatment of Dilatometry Data*

Six steps are used in extracting information from dilatometry data to construct a master sintering curve. These

Table II. Manipulation Procedure from Dilatometry Data to Density History

Step	Calculated Value	Equation	Explanation
1	ε_d	$\varepsilon_d = \dfrac{L - L_0}{L_0}$	engineering strain from dilatometry test
2	ε'_d	$\varepsilon'_d = \dfrac{\varepsilon_d - \delta}{1 + \delta}$	elimination nonzero initial value in dilatometry data
3	ε''_d	$\varepsilon''_d = \varepsilon'_d - \alpha_m \rho^{1/3}(T - T_0)$	consideration of the effect of thermal expansion
4	ρ	$\rho = \dfrac{\rho_0}{(1 + \varepsilon''_d)^3}$	calculation of relative density from engineering strain data
5	ρ'	$\rho'_{i+1} = \rho_i$ if $\rho_{i+1} > \rho_i$ $\rho'_{i+1} = \rho_{i+1}$ otherwise	requirement of nondecreasing function
6	ρ''	$\rho''_{i+1} = 1$ if $\rho_{i+1} > 1$ $\rho''_{i+1} = \rho_{i+1}$ otherwise	requirement of maximum value of 1

steps are detailed in Table II. Through this manipulation of the dilatometry data, the thermal expansion effects are removed, thus yielding an accurate measure of relative density during sintering. Table III shows the thermal expansion coefficients used for each material in this study. In addition, this manipulation removes the effects of the following circumstances on dilatometer shrinkage measurements: (1) a nonzero initial value, (2) nondecreasing function, and (3) maximum value of one. Taking these factors into account reduces the error in predicting relative density from experimental data. The sigmoid function, which is used as a model function for the master sintering curve,[7,10] is compliant to all of these considerations.

C. *Construction of Master Sintering Curve*

1. *Finding the apparent activation energy for sintering*

The apparent activation energy for sintering defines the master sintering curve. It is conventionally obtained using shrinkage data from either isothermal or constant-heating-rate experiments. Comparing the activation energy derived from experimental data to published values for activation energies associated with specific diffusional paths, *i.e.,* volume, surface, or grain boundary diffusion, can help in identifying the primary diffusional mechanisms responsible for sintering.[12,20,21] An alternative method is to estimate the apparent sintering activation energy on the basis of the master sintering curve itself.[7,10,11] In this study, the apparent sintering activation energy is obtained by minimizing the normalized dimensionless mean residual square, defined as the following equation:

$$\text{Mean residual square} \equiv \sqrt{\frac{1}{\rho_s - \rho_0}\int_{\rho_0}^{\rho_s} \frac{\sum_{i=1}^{N}\left(\dfrac{\Theta_i}{\Theta_{\text{avg}}} - 1\right)^2}{N} d\rho} \qquad [5]$$

where N is the number of experimental data points, and Θ_{avg} is the average of all Θ_i over N. The trapezoidal integration rule and bisection method are used as numerical methods in this error minimization.

Figures 2(a) and (b) are plots of mean residual square *vs* the apparent sintering activation energy, with the minimum mean residual square value corresponding to the apparent sintering activation energy for 17-4 PH stainless steel and W-Ni-Fe (95:3:2), respectively. To use this minimization method to determine the apparent activation energy, generally, three different constant heating rates, or isothermal hold temperatures, are needed. For the other materials in this study, the diversity of the experimental data available did not allow for calculation of the apparent sintering activation energy. In these cases, the grain boundary diffusion activation energy was used because this is the predominant diffusional mechanism responsible for sintering of these materials.[12] The apparent sintering activation energies used in this study are summarized in Table IV.

Table III. Thermal Expansion Coefficient Used in Dialatometry Data Manipulation

Materials	Thermal Expansion Coefficient (K^{-1})	Test Method
17-4PH SS	1.37×10^{-5}	dilatometry
316L SS	1.31×10^{-5}	dilatometry
Nickel	1.73×10^{-5}	Ref. [12]
W-Ni-Fe (95:3:2)	1.46×10^{-6}	dilatometry
W-Ni-Fe (88:8.4:3.6)	1.07×10^{-6}	dilatometry

The value of the minimum normalized dimensionless mean residual square reflects the quality of experimental data or the applicability of master sintering curve to a given sintering system, with a low value showing a closer correlation.

2. *Construction of the master sintering curve*

A master sintering curve is constructed by plotting the relative density, extracted from dilatometry data as described in Section II–B, *vs* the natural logarithm of the work of sintering, calculated by Eq. [1]. The apparent sintering activation energy used in this calculation is material dependent (Table IV). Figures 3(a) through (h) show master sintering curves for the systems investigated.

D. *Modeling of Master Sintering Curve by Sigmoid Function*

1. *Defining the shape of the master sintering curve*

Su and Johnson[6] suggested that a polynomial function can be used to describe the master sintering curve relationship

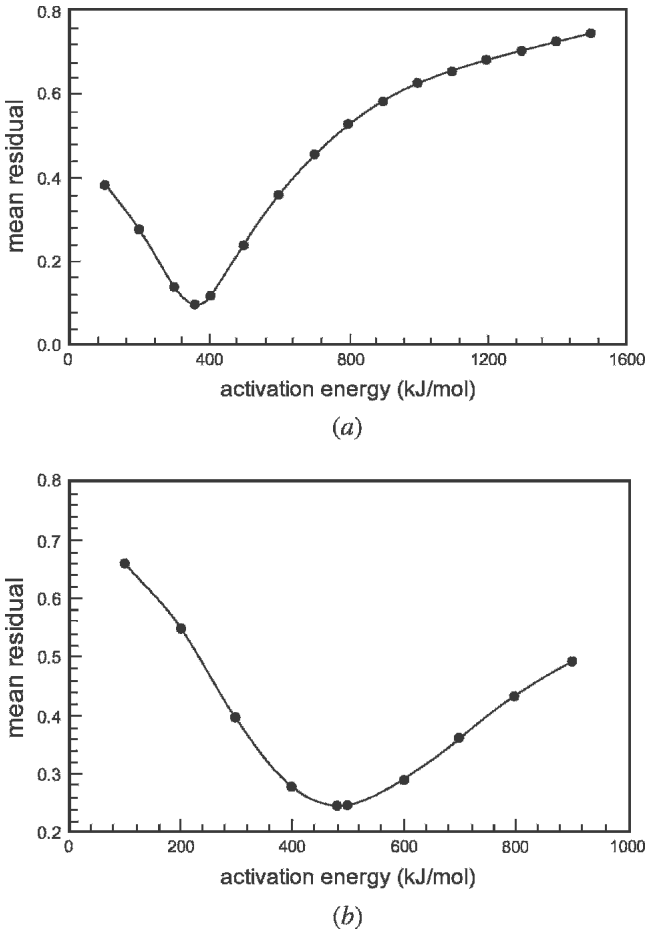

Fig. 2—Mean residual *vs* apparent sintering activation energy plot: (*a*) 17-4 PH stainless steel and (*b*) W-Ni-Fe (95:3:2).

between the relative density and the natural logarithm of the work of sintering. However, we found that a sigmoid function best describes this relationship:

$$\rho_s = \rho_0 + \frac{1-\rho_0}{1+\exp\left(-\frac{(\ln\Theta - a)}{b}\right)} \qquad [6]$$

This form of the sigmoid function is similar to that advocated by Teng *et al.*,[10] with the constants *a* and *b* in Eq. [6] obtained by curve fitting. The parameter *a* coincides with the point of inflection of the curve, while the parameter *b* is the slope of the linearized curve. Teng *et al.*[10] included additional parameters to define his sigmoidal curve; however, these parameters are incorporated into the model presented here by making the following assumptions: the work of sintering is indirectly proportional to the final density (*i.e.,* Teng *et al.*'s parameter *c* is equal to unity), and the nominator of the second term in the sigmoid function (*i.e.*, Teng *et al.*'s parameter *a*) is equal to $1 - \rho_0$.

The generalized Newtonian method is the numerical method used to fit the experimental data to the sigmoid function given in Eq. [6] by minimizing the following normalized dimensionless error:

Table IV. Apparent Sintering Energy Used in Construction of Master Sintering Curve

Materials	Apparent Sintering Activation Energy (KJ/mol)	Mean Residual
17-4PH SS	360	0.096
316L SS	167	[12]
W-Ni-Fe (95:3:2)	482	0.240
W-Ni-Fe (88:8.4:3.6)	250	—
Niobium	263	12
Molybdenum	418	12
Nickel	108	12

$$\text{Error} = \sqrt{\frac{1}{\ell n\Theta_s - \ell n\Theta_0}\int_{\ell n\Theta_0}^{\ell n\Theta_s}\frac{\sum_{i=1}^{N}\left(\frac{\rho_i}{\rho_s}-1\right)^2}{N}\,d\ell n\Theta} \qquad [7]$$

Figure 4 is the flowchart detailing the algorithm used to convert dilatometer data into the final sigmoid curve function describing the master sintering curve. The value of the normalized dimensionless error proposed in this study reflects the accuracy of sigmoid curve prediction for a given sintering system, with a lower value indicating less error. In Figures 3(a) through (h), dotted lines indicate curve-fit sigmoid function prediction models for the sintering systems under investigation. Table V summarizes the sigmoid function parameters *a* and *b* from Eq. [6] and all errors obtained from Eq. [7] for the material systems studied.

2. *Normalization of relative density*

One of the challenges is in comparing materials where the initial relative densities differ.[7,9] German[12] suggests using the densification parameter Ψ to overcome this type of problem. In terms of the symbols used in this study, it is defined as

$$\Psi = \frac{\rho_s - \rho_0}{1-\rho_0} \qquad [8]$$

Equation [8] is a linear transformation of the relative density variation from $\rho_0 \rightarrow 1$, to a densification parameter variation from $0 \rightarrow 1$. Therefore, Ψ gives an indication of the degree to which a green compact has approached its theoretical limit, the degree of sintering.

Applying this transformation to the experimental data set allows for general comparison of all of the master sintering curves, as shown in Figure 5.

IV. DISCUSSION

In order to verify the methods for obtaining and constructing the master sintering curve, existing data for alumina sintered in a conventional furnace at low oxygen pressure was examined. Johnson[21] calculated an activation energy of 488 ± 20 kJ/mol for alumina from Arrenhius slope analysis of shrinkage data, and later, using the master sintering curve approach to find the activation energy for sintering, found the minimum mean of residual squares to

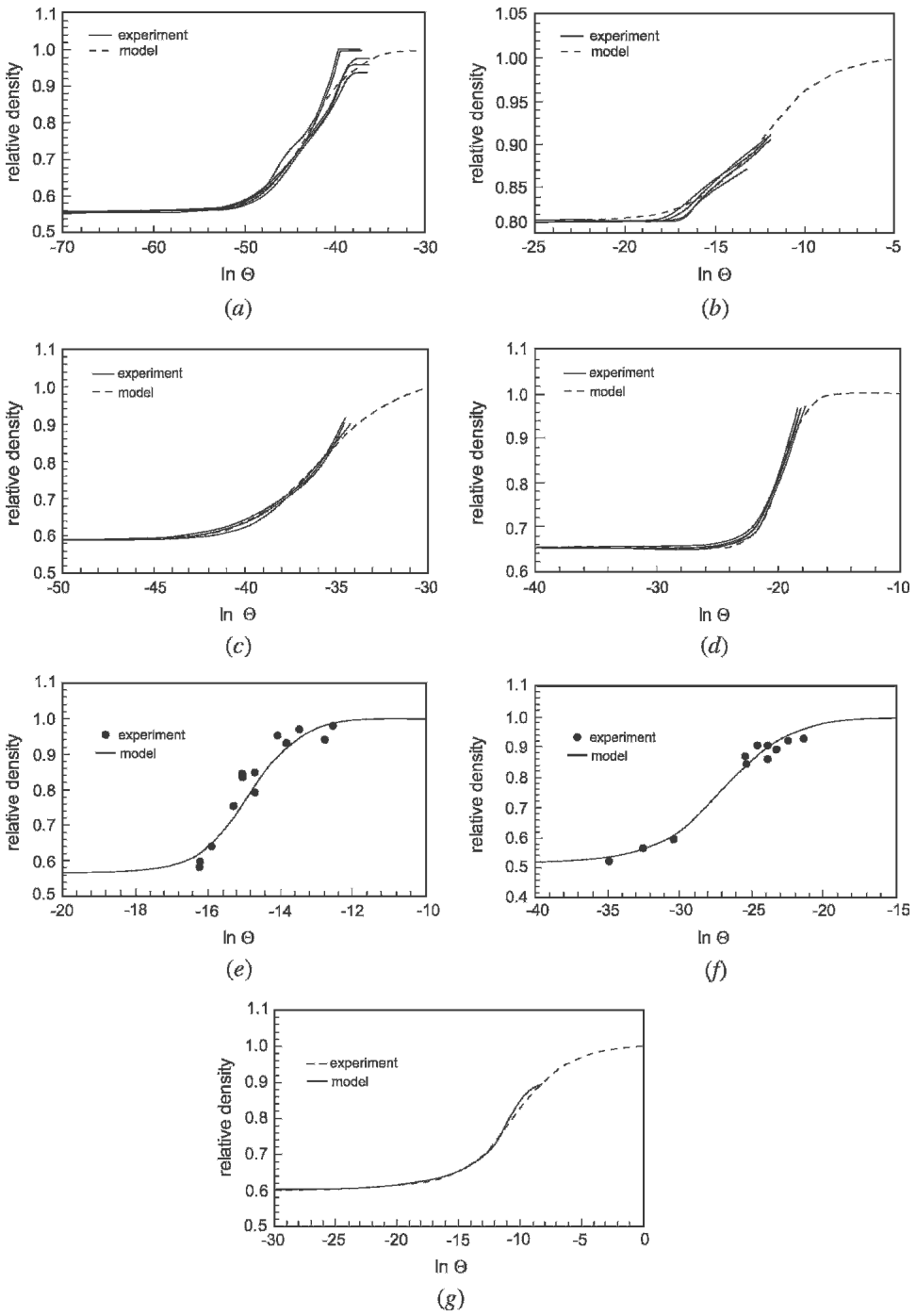

Fig. 3—Master sintering curve with sigmoid functions plot for (*a*) 17-4 PH stainless steel, (*b*) 316L stainless steel, (*c*) W-Ni-Fe (95:3:2), (*d*) W-Ni-Fe (88:8.4:3.6), (*e*) niobium, (*f*) molybdenum, and (*g*) nickel.

occur at an activation energy of 440 kJ/mol for the same data set.[7] Teng *et al.*[10] calculated an activation energy of 450 kJ/mol for the same alumina data. According to our calculations, we found the activation energy to be 452 kJ/mol, by using data taken from the reported shrinkage curves.[7] German[12] gives the theoretical value for grain boundary activation energy for alumina as 477 kJ/mol.[12] These values are all within a reasonable range of the theoretical value for grain boundary activation energy to conclude that this is the primary densification mechanism for this system. The differences in the sintering activation energy calculated by the master sintering curve analyses can be attributed to statistical differences relating to the size of the database used to calculate the curve, as well as the accuracy of the data. Thus, the activation energy for sintering determined from master sintering curve only gives an indication of the primary densification mechanism. Furthermore, the accuracy of the calculated sintering activation energy is only powerful in its density prediction capacity when teamed with the related master sintering curve function.

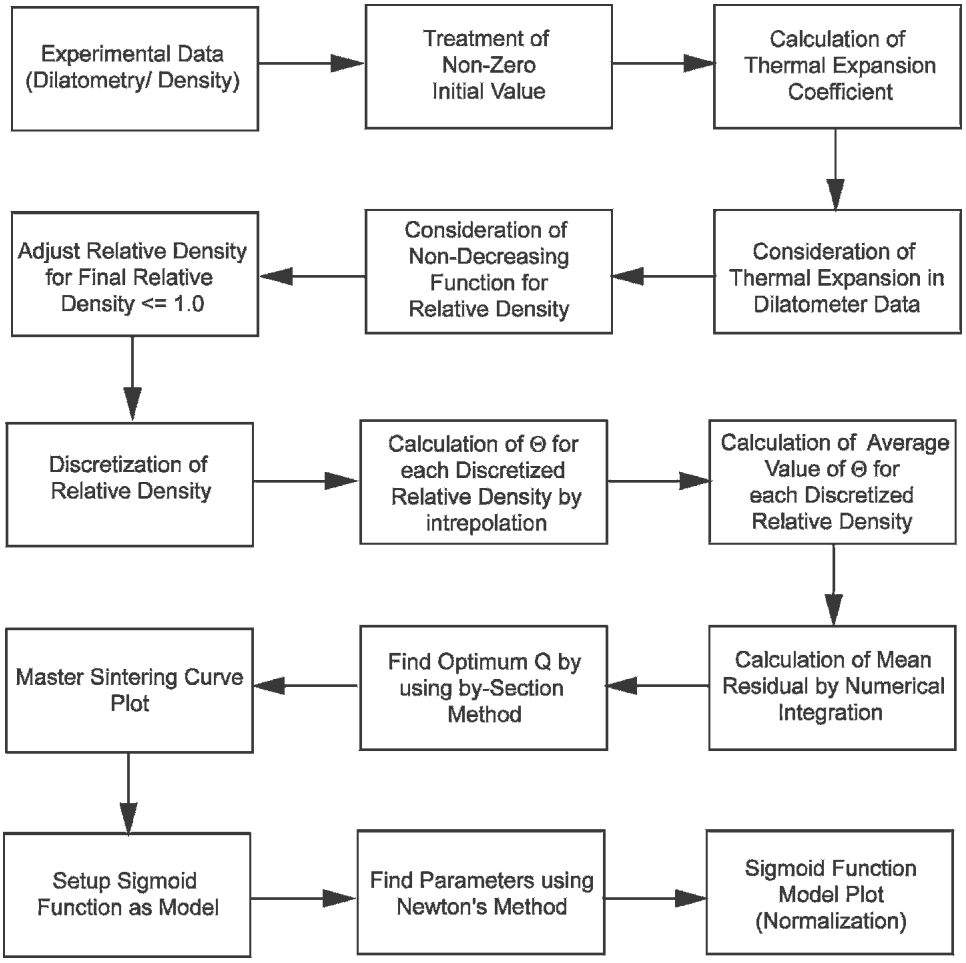

Fig. 4—Overall algorithm for construction of master sintering curve.

Table V. Sigmoid Function Parameters and Errors Obtained by Curve Fitting Processes

Materials	Initial Relative Density	Parameter *a*	Parameter *b*	Error ($\times 10^{-3}$)
17-4PH SS	0.55	−30.4	1.89	10.6
316L SS	0.81	−12.4	1.81	3.34
W-Ni-Fe (95:3:2)	0.50	−35.8	2.01	3.55
W-Ni-Fe (88:8.4:3.6)	0.65	−19.9	1.01	5.66
Niobium	0.57	−14.5	0.718	61.9
Molybdenum	0.52	−27.0	2.38	26.4
Nickel	0.60	−10.6	2.36	5.20

A similar comparative analysis was performed for yittria-stabilized zirconia.[10] Teng *et al.* calculated a sintering activation energy of 660 kJ/mol for these data, while we calculated 607 kJ/mol. The difference in the activation energies can be attributed to the size of the sintering data database and the sigmoid function describing the master sintering curve. These two examples show that the methods we use yield results comparable to existing analyses and data.

For the cases of 17-4 PH stainless steel and the 95 pct tungsten heavy alloy, the apparent activation energy for sintering was calculated using the master sintering curve. For 17-4 PH stainless steel, the calculated apparent activation energy for sintering is 360 kJ/mol, and in the case of the 95 pct tungsten heavy alloy, it is 482 kJ/mol. Kwon *et al.* calculated the activation energy for 17-4 PH stainless steel as 328 kJ/mol.[22] The grain boundary diffusion activation energy for pure tungsten is 385 kJ/mol, the activated sintering activation energy for tungsten mixed with iron is 380 kJ/mol, and when it is mixed with nickel, it is around 300 kJ/mol.[12]

For 17-4 PH stainless steel, the apparent activation energy for sintering calculated from the master sintering curve is close enough to the reported grain boundary activation energy to confirm that grain boundary diffusion is the main sintering densification mechanism. The difference between

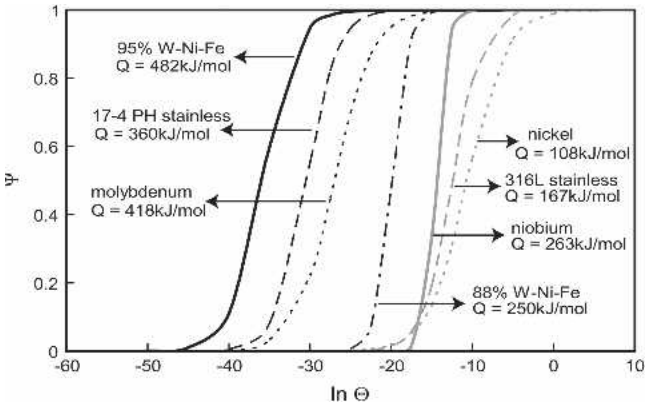

Fig. 5—Normalized master sintering curves for materials.

the two values can be attributed to statistical and empirical influences.

When tungsten is sintered in the presence of nickel and iron, these alloying elements act as sintering activators, lowering the activation energy for sintering.[12] However, the sintering activation energy we calculate for the 95 pct tungsten heavy alloy is 25 pct higher than the grain boundary diffusion activation energy for pure tungsten. The difference in the reported and calculated activation energies can be linked to processing conditions that favor surface diffusion.

In both cases, the mean particle size was less than 10 μm and the injection molded samples were thermally debound before sintering. The combination of small particle size and exposure to low temperatures during debinding promotes initial stage sintering by surface diffusion. During initial stage sintering, minimal densification occurs, but there is a significant change in the pore structure of the compact as necks grow between particles. The result of the change in particle and pore morphology could result in an increase in the apparent activation energy for sintering (densification). Thus, surface diffusion influences the calculation of the apparent activation energy for sintering when using the master sintering curve method,[9] causing the apparent activation energy for sintering to differ from the activation energy for the main diffusional sintering mechanism, either grain boundary or volume diffusion.

In the cases of 17-4 PH and 95 pct tungsten heavy alloy, the sintering kinetics may be masked by the presintering events, but this does not distract from the capability of the master sintering curve as a density prediction model. The curves constructed using the calculated activation energies show close correlation to the experimental data.

For the remaining materials, 316L stainless steel, 88 pct tungsten heavy alloy, niobium, molybdenum, and nickel, the estimated master sintering curves, constructed using the grain boundary diffusion activation energy, have correlations to the experimental data with less than 1 pct error from continuous dilatometer data and less than 7 pct error from furnace data.

Using the densification parameter instead of the relative density as a monitor allows for the various materials studied to be analyzed relative to each other, regardless of their differing initial density values, as shown in Figure 5. As the work of sintering, Θ represents the energy required to densify a porous body, with a low value for Θ indicating a high amount of energy. From Figure 5, it is clear that 10-μm nickel powder requires the least amount of work to densify, while a 95 pct tungsten heavy alloy requires the most. This is intuitive as the temperature at which a material densifies is linked to its melting temperature, and to the particle size. Nickel has a melting temperature of 1453 °C, while pure tungsten melts only at 3410 °C. Further insight into the relative sintering kinetics of the various material systems can be gained from examining the slope, or width, of the sigmoid curves. The 95 pct tungsten heavy alloy system studied here does not have as steep as slope, or as wide a range as, for instance, the niobium studied. This would indicate that the densification of the tungsten heavy alloy occurs more slowly, once the sintering temperature is reached, than that for niobium and that it takes more effort to reach full density toward the end of the sintering cycle in the tungsten heavy alloy. This probably reflects grain boundary and pore attachment phenomena in the tungsten heavy alloy system. It should be noted that even though the data have been normalized through the densification parameter, the effects of particle size and consolidation technique are still included in the analysis; densification is not dependent on the material characteristics alone.

V. CONCLUSIONS

The master sintering curve concept has been applied to several powder metal systems, consolidated and sintered in a variety of ways. Using published values for grain boundary diffusion activation energy allows for creation of master sintering curves with sufficient accuracy that the model can be used as a guideline to analyze sinter cycle design. Factors such as particle size and process route have significant influence on the master sintering curve; thus, if an accurate model is needed, it is necessary to calculate the activation energy from constant heating rate experiments conducted on the specific powder material system.

ACKNOWLEDGMENTS

This work was conducted at the Center for Innovative Sintered Products, The Pennsylvania State University, partially funded by ATP/NIST Project No. 70NANB0H3019 investigating sinter models for the production of large powder injection molded parts and the Brush Chair. The publication of this work was sponsored by the Center for Advanced Vehicular Systems, Mississippi State University.

NOMENCLATURE

ρ	relative density
T	temperature (K)
t	time (s)
R	universal gas constant, 8.314 J/mol·K
Q	activation energy for sintering (J/mol)
L	length of compact (m)
γ	surface energy (J/m^2)
k	Boltzmann's constant, $1.381 \cdot 10^{-23}$ J/K
Γ	lumped scaling factor

D	diffusivity (m^2/s)
G	grain size (m)
Ω	atomic volume (m^3)
Θ	work-of-sintering (s/K)
Ψ	densification parameter

Subscripts

avg	average
v	volume
b	grain boundary
0	initial
s	sintered

REFERENCES

1. J.H. Flynn: *Thermochim. Acta*, 1997, vol. 300, pp. 83-92.
2. G.C. Kuczynski: *TMS-AIME*, 1949, vol. 185 (2), pp. 169-78.
3. R.L. Coble: *J. Am. Ceram. Soc.*, 1958, vol. 41 (2), pp. 55-62.
4. A.F. Ashby: *Acta Metall.*, 1974, vol. 22, pp. 275-89.
5. G.A. Shoales and R.M. German: *Metall. Mater. Trans. A*, 1999, vol. 30A, pp. 465-70.
6. D.L. Johnson and H. Su: *Advances in Powder Metallurgy and Particulate Materials,* 1997, vol. 2, pp. 14.115-14.121.
7. H. Su and D. Lynn Johnson: *J. Am. Ceram. Soc.*, 1996, vol. 79 (12), pp. 3211-17.
8. H.R. Shercliff and M.F. Ashby: *Acta Metall. Mater.*, 1990, vol. 38 (10), pp. 1803-12.
9. D.L. Johnson: *Proc. Sintering*, www.mri.psu.edu/conferences/sint03/#p1, MRI, The Pennsylvania State University, University Park, PA, 2003.
10. M.-H. Teng, Y.-C. Lai, and Y.-T. Chen: *Western Pacific Earth Sci.*, 2002, vol. 2 (2), pp. 171-80.
11. T.R.G. Kutty, K.B. Khan, P.V. Hegde, A.K. Sengupta, S. Majumdar, and H.S. Kamath: *Sci. Sintering*, 2003, vol. 35, pp. 125-32.
12. R.M. German: *Sintering Theory and Practice*, Wiley & Sons, New York, NY, 1996, pp. 78-95.
13. J.D. Hansen, R.P. Rusin, M.-H. Teng, and D. Lynn Johnson: *J. Am. Ceram. Soc.*, 1992, vol. 75 (5), pp. 1129-35.
14. I. Kaur, W. Gust, and L. Kozma: *Handbook of Grain and Interphase Boundary Diffusion Data*, University of Stuttgart, Stuttgart, Germany, 1996, vol. 1.
15. Y. Wu, D. Blaine, B. Marx, C. Schlaefer, and R.M. German: *Metall. Mater. Trans. A*, 2002, vol. 33A, pp. 2185-94.
16. R. Bollina: Master's Thesis, The Pennsylvania State University, University Park, PA, 2002, pp. 24-54.
17. G. Aggarwal: Master's Thesis, The Pennsylvania State University, University Park, PA, 2003, pp. 28-36.
18. J.D.S. Gurosik: Master's Thesis, The Pennsylvania State University, University Park, PA, 2003, pp. 48-82.
19. D.C. Blaine: Ph.D. Thesis, The Pennsylvania State University, University Park, PA, 2004, pp. 65-82.
20. J. Wang and R. Raj: *J. Am. Ceram. Soc.*, 1990, vol. 73 (5), pp. 1172-75.
21. H. Su and D.L. Johnson: *J. Am. Ceram. Soc.*, 1996, vol. 79 (12), pp. 3199-210.
22. Y.-S. Kwon, Y. Wu, P. Suri, and R.M. German: *Metall. Mater. Trans. A*, 2004, vol. 35A, pp. 257-60.